

## Attempts to chemically investigate element 112

By R. Eichler<sup>1,2,\*</sup>, W. Bröchle<sup>3</sup>, R. Buda<sup>4</sup>, S. Bürger<sup>4</sup>, R. Dressler<sup>1</sup>, Ch. E. Düllmann<sup>5,6,###</sup>, J. Dvorak<sup>7</sup>, K. Eberhardt<sup>4</sup>, B. Eichler<sup>1</sup>, C. M. Folden III<sup>5,6</sup>, H. W. Gäggeler<sup>1,2</sup>, K. E. Gregorich<sup>5</sup>, F. Haenssler<sup>2</sup>, D. C. Hoffman<sup>5,6</sup>, H. Hummrich<sup>4</sup>, E. Jäger<sup>3</sup>, J. V. Kratz<sup>4</sup>, B. Kuczewski<sup>4</sup>, D. Liebe<sup>4</sup>, D. Nayak<sup>8</sup>, H. Nitsche<sup>5,6</sup>, D. Piguet<sup>1</sup>, Z. Qin<sup>9</sup>, U. Rieth<sup>4,####</sup>, M. Schädel<sup>3</sup>, B. Schausten<sup>3</sup>, E. Schimpf<sup>3</sup>, A. Semchenkov<sup>3,7</sup>, S. Sovarna<sup>2</sup>, R. Sudowe<sup>5</sup>, N. Trautmann<sup>4</sup>, P. Thörle<sup>4</sup>, A. Türler<sup>7</sup>, B. Wierczinski<sup>7</sup>, N. Wiehl<sup>4</sup>, P. A. Wilk<sup>7,#</sup>, G. Wirth<sup>3</sup>, A. B. Yakushev<sup>7</sup> and A. von Zweidorf<sup>3,##</sup>

<sup>1</sup> Labor für Radio- und Umweltchemie, Paul Scherrer Institut, 5232 Villigen, Switzerland

<sup>2</sup> Departement für Chemie und Biochemie, Universität Bern, 3012 Bern, Switzerland

<sup>3</sup> Gesellschaft für Schwerionenforschung mbH, 64291 Darmstadt, Germany

<sup>4</sup> Institut für Kernchemie, Universität Mainz, 55099 Mainz, Germany

<sup>5</sup> Nuclear Science Division, Lawrence Berkeley National Laboratory, Berkeley, CA 94720, USA

<sup>6</sup> Department of Chemistry, University of California, Berkeley, CA 94720, USA

<sup>7</sup> Institut für Radiochemie, Technische Universität München, 85748 Garching, Germany

<sup>8</sup> Chemical Sciences Division, Saha Institute of Nuclear Physics, 700064 Kolkata, India

<sup>9</sup> Institute of Modern Physics, Chinese Academy of Sciences, 730000 Lanzhou, P.R. China

(Received September 16, 2005; accepted November 18, 2005)

### *Adsorption / Transactinides / Element 112 / Thermochromatography*

**Summary.** Two experiments aiming at the chemical investigation of element 112 produced in the heavy ion induced nuclear fusion reaction of  $^{48}\text{Ca}$  with  $^{238}\text{U}$  were performed at the Gesellschaft für Schwerionenforschung (GSI), Darmstadt, Germany. Both experiments were designed to determine the adsorption enthalpy of element 112 on a gold surface using a thermochromatography setup. The temperature range covered in the thermochromatography experiments allowed the adsorption of Hg at about 35 °C and of Rn at about –180 °C. Reports from the Flerov Laboratory for Nuclear Reactions (FLNR), Dubna, Russia claim production of a 5-min spontaneous fission (SF) activity assigned to  $^{283}112$  for the  $^{238}\text{U}(^{48}\text{Ca},3n)^{283}112$  reaction. Hence, Experiment I was designed to detect spontaneously fissioning (SF) isotopes of element 112 with half-lives ( $t_{1/2}$ ) longer than about 20 s. 11 high-energy events were detected. 7 events exhibit a deposition pattern resembling a chromatographic peak in the vicinity of Rn deposition. However, the energy of the events observed in Experiment I was lower than expected for a SF-decay of  $^{283}112$ . Therefore, these events could not be unambiguously attributed to the decay of  $^{283}112$ . In contradiction with earlier publications newer reports from FLNR Dubna claim that  $^{283}112$  decays by  $\alpha$ -particle emission ( $E_\alpha = 9.5$  MeV) with  $t_{1/2} = 4$  s followed by a SF-decay of  $^{279}\text{Ds}$  ( $t_{1/2} = 0.2$  s). Therefore, Experiment II was designed to be sensitive to both claimed decay properties of  $^{283}112$ . However, during

this experiment neither short  $\alpha$ -SF correlations nor SF coincidences were detected. The conclusion is that  $^{283}112$  was not unambiguously detected, neither in Experiment I nor in Experiment II.

### 1. Introduction

The prediction of enhanced nuclear stability around the doubly magic spherical nucleus  $^{298}114$  [1, 2] initiated an experimental rush for super heavy elements (SHE). Various radiochemical separation procedures have been developed and applied for the extensive SHE search in nature (for review see [3, 4]) and also for the search within the products of nuclear transfer or fusion reactions (see, *e.g.*, [5–7]).

Between 1994 and 1996, the discoveries of Ds, Rg, and element 112 were announced at the GSI Darmstadt (for review see [8]). However, only very short-lived neutron deficient isotopes could be produced in fusion reactions using Pb and Bi targets. Starting in 1999, the discovery of more than 30 new isotopes from Rf up to element 118 has been reported at the FLNR Dubna, Russia (for review see [9]). These new isotopes appear to be accessible in  $^{48}\text{Ca}$  induced nuclear fusion reactions with actinide targets such as  $^{238}\text{U}$ ,  $^{242,244}\text{Pu}$ ,  $^{243}\text{Am}$ ,  $^{245,248}\text{Cm}$ , or  $^{249}\text{Cf}$ . The observation of lifetimes ranging from several seconds up to minutes for isotopes of elements 112 and 114 indicates the close proximity of the so called “island of stability” of SHE. The proof of the mass and the nuclear charge of these new isotopes is difficult because all observed decay chains consist of previously unknown nuclides. The data available on the decay properties and production rates of  $^{283}112$  in  $^{48}\text{Ca}$  induced nuclear fusion reactions with actinide targets are conflicting. Experiments at the electrostatic separator VASSILISSA at FLNR Dubna indicated the production of the isotope  $^{283}112$  in the nuclear reaction of  $^{48}\text{Ca}$  on  $^{238}\text{U}$  with a production cross section of about  $3_{-2}^{+4}$  pb [10–12].  $^{283}112$  was claimed to decay exclu-

\* Author for correspondence (E-mail: robert.eichler@psi.ch)

# Present address: Lawrence Livermore National Laboratory, Livermore, CA 94550, USA.

## Present address: Institute for Transuranium Elements, 76125 Karlsruhe, Germany.

### Present address: <sup>3</sup>

#### Present address: Institut für Fischereiökologie, 20539 Hamburg, Germany

sively by spontaneous fission (SF) with a half-life of about 5 min. It was also identified as  $\alpha$ -decay product of  $^{287}114$  produced in the reaction of  $^{48}\text{Ca}$  with  $^{242}\text{Pu}$  [10, 11]. Later, in a series of experiments at the Dubna Gas-Filled Recoil Separator (DGFRS) at FLNR Dubna,  $^{283}112$  was claimed to decay by  $\alpha$ -emission ( $E_\alpha = 9.5$  MeV) with a half-life of about 4 s to  $^{279}\text{Ds}$ , which then decayed mainly by SF (90%) with a half-life of about 0.2 s [9]. The production cross section was estimated to  $2.5_{-1.1}^{+1.8}$  pb.  $^{279}\text{Ds}$  was reported to also have a  $\sim 10\%$   $\alpha$ -branch ( $E_\alpha = 9.7$  MeV). Other independent experiments aiming at the observation of  $^{283}112$  in the  $^{48}\text{Ca}$  on  $^{238}\text{U}$  reaction at the Lawrence Berkeley National Laboratory (LBNL), Berkeley, USA using the Berkeley Gas-filled Separator (BGS) were unable to confirm the observation of  $^{283}112$  [13, 14].

The reported lifetimes and formation cross sections of picobarns would allow a chemical investigation of these elements. Apart from important basic chemical information the determination of chemical properties of element 112 will provide a clear indication of the atomic number  $Z$  for verification of reports of nuclear properties. These chemical investigations are complicated by the uncertainty in the magnitude of relativistic effects which are induced by the high nuclear charge of SHE. These effects are expected to strongly influence the electronic structure of atoms of SHE and hence their chemical behavior [15–19]. The relativistic contraction of the  $s$  and  $p_{1/2}$  electron orbitals leads to a stabilization of the elemental state of atoms with valence electrons occupying these orbitals. Element 112 with an expected electronic ground state configuration  $[\text{Rn}]5f^{14}6d^{10}7s^2$  is predicted to reveal a more inert chemical character and also enhanced volatility compared to its lighter homologue Hg [15]. A higher volatility compared to Hg can also be expected from the trends in group 12 of the periodic table [20]. However, comparable to its lighter homologue Hg, element 112 is expected to reveal metallic properties in contact with noble metals [21–23]. Recent density functional calculations indicate that the screening of the nuclear charge due to the contraction of the  $7s$  orbital may lead to weaker bonding of the electrons in the  $6d$  shell [18, 19]. Thus, a behavior very similar to that of Hg is predicted. The best way currently known to assess such a broad range of properties for element 112 is the investigation of its adsorption interaction with noble metal surfaces (for a review see [24]).

Previous attempts to measure the adsorption properties of element 112 in its elemental state on gold and palladium surfaces at room temperature were performed at FLNR Dubna in 2000 and 2001 [25, 26]. In the experiment in 2000 no SF decays were observed. In the second experiment in 2001,  $^{238}\text{U}_3\text{O}_8$  targets were irradiated with a beam dose of  $2.8 \times 10^{18}$   $^{48}\text{Ca}$  particles at an energy of about 231 MeV in the center of the target. The volatile products were flushed through thin Teflon<sup>®</sup> capillaries to a gold coated detector array which served as an isothermal adsorption chromatography column held at room temperature. Downstream of the detector, a gas ionization chamber was connected. During the experiment 8 high-energy events were detected in this ionization chamber at various gas flow rates, at an expected background of 1 event. The assignment of these events to SF was corroborated by measurement of prompt

neutrons using a  $^3\text{He}$ -neutron counter array placed around the entire setup. The observed events were attributed to the decay of  $^{283}112$ , based on the decay data available at that time [10, 11]. The non-observation of element 112 on the gold coated solid state detectors at room temperature indicated a non Hg-like behavior. The adsorption enthalpy of element 112 on gold ( $-\Delta H_{\text{ads}}^{\text{Au}}(112)$ ) was estimated as  $\leq 60$  kJ/mol. After the reports on different decay properties for  $^{283}112$  [9] it was evaluated whether the 8 SF-decays observed could originate from the decay of the  $^{283}112$   $\alpha$ -decay daughter  $^{279}\text{Ds}$ . Due to its low volatility and its short half-life,  $^{279}\text{Ds}$  should not have been transported to the ionization chamber. Severe transport losses had to be considered for the short-lived 4-s  $^{283}112$ . Therefore, a higher production cross section of  $> 7$  pb had to be concluded for  $^{283}112$  to attribute some of the SF-events observed in the gas ionization chamber to the decay of  $^{279}\text{Ds}$  [27].

Here we describe two experimental attempts performed in 2003 (Experiment I) and 2004 (Experiment II) at GSI Darmstadt aiming at the confirmation of these first chemical investigations of element 112 by quantifying its adsorption properties on gold in a thermochromatographic setup. Results from both experiments were already partly presented in [28, 29].

## 2. Experiments

### 2.1 Experiment I

An experimental technique based on the principle of the *In-situ* Volatilization and On-line detection (IVO) was developed for thermochromatographic gas adsorption investigations of very volatile species [30, 31]. This system was successfully applied to the first chemical characterization of hassium (element 108) [32]. The entire setup has been modified to adapt it to the needs of the chemical investigation of element 112. The principal design has been described in [28, 33, 34].

The nuclear reaction products were thermalized in a recoil chamber mounted behind the target assembly and flushed with a carrier gas (1 l/min He). This chamber was completely made out of quartz to avoid any losses of element 112 due to adsorption on metal surfaces. Only a small area in the vicinity of the graphite beam stop was not covered with quartz. Most non-volatile reaction products were retained in this chamber. Aerosol particles produced by beam induced sputtering processes were stopped on a quartz-wool filter kept at a temperature of 850 °C behind the outlet of the recoil chamber. In test experiments with  $^{156}\text{Yb}$ , serving as a model isotope for heavy actinides, separation factors of  $> 10^6$  were determined [34]. The overall transport time to the detection system was about 25 s including the transport through a 10-m long perfluoroalkoxy (PFA<sup>®</sup>) capillary (*i.d.* 2 mm) and through a subsequent Ta/Ti getter, kept at 1000 °C. The getter acted as a trap for traces of water and oxygen in the carrier gas. The Cryo-On-Line Detector (COLD) detection system consisted of an array of 32 silicon PIN-photodiodes ( $10 \times 8.9$  mm<sup>2</sup> active area) mounted in a Teflon<sup>®</sup> coated copper channel at a distance of 1.6 mm opposite to a gold covered surface, forming a rectangular gas chromatographic column. A temperature gradient from +35 °C to –185 °C

was established along this chromatographic channel by heating the inlet with a thermostat and by cooling the outlet with a liquid nitrogen cryostat. The channel was placed in a steel housing evacuated to  $< 1$  mbar. While the temperature gradient was established, the channel started leaking He until the same pressure was reached in the housing as inside the channel ( $\sim 1.1$  bar). The size of the PIN diodes allowed for a lateral resolution of 1 cm corresponding to a temperature resolution of about  $5^\circ\text{C}$ . The event-by-event spectroscopy with PIN diodes allowed for on-line identification of SF- and  $\alpha$ -decaying nuclides deposited on the gold surface in a  $2\pi$ -detection geometry [35]. The experimental setup was tested and optimized with single atoms of short-lived isotopes of elemental Hg and Rn [33, 34, 36]. An overall efficiency of about 70% was determined for  $^{185}\text{Hg}$  ( $t_{1/2} = 49$  s) considering transport losses and deposition characteristics in the COLD. The transport efficiency for  $^{220}\text{Rn}$  ( $t_{1/2} = 55.6$  s) was about 75%, but only about 50% of the transported Rn were deposited in the COLD.

At the UNILAC accelerator at GSI Darmstadt, an uranium oxide target ( $1.6\text{ mg/cm}^2$   $^{238}\text{U}$ ) prepared by molecular plating was irradiated with an average intensity of about  $1.9 \times 10^{12}$  particles  $\text{s}^{-1}$  of  $^{48}\text{Ca}$  using a rotating actinide target assembly. This target setup is equipped with a synchronously rotating vacuum window and target wheel. Hence, it is able to accept the high intensity pulsed heavy ion beams delivered from the UNILAC accelerator.  $^{141}\text{Nd}$  ( $20\ \mu\text{g/cm}^2$ ) was added to one segment of the rotating target wheel to produce the  $\alpha$ -decaying nuclide  $^{185}\text{Hg}$ . Various isotopes of Rn (*e.g.*,  $^{220}\text{Rn}$ ) were produced in nuclear transfer reactions of  $^{48}\text{Ca}$  with  $^{238}\text{U}$ . Thus, Rn and Hg were studied simultaneously with element 112 throughout the entire experiment.

The uranium targets were prepared by the molecular plating technique. The uranium was deposited as uranyl nitrate on the beryllium target backings. During the first hours of irradiation the color of the target material was observed to change from yellow-green to black. Hence, it was assumed that the initial uranyl compound was converted to  $\text{U}_3\text{O}_8$  by the interaction with the beam.

Prior to Experiment I, the projectile energy distribution in the target material was measured with a PIPS detector placed at the position of the beam stop behind the target setup. At first, the UNILAC beam ( $346.2\text{ MeV}$ ) was directed onto the detector at a significantly reduced intensity. In two subsequent measurements, a Be-window ( $3.81\text{ mg/cm}^2$ ) and a combination of Be-window ( $3.81\text{ mg/cm}^2$ ) and the Be target backing ( $1.96\text{ mg/cm}^2$ ) were placed in front of the detector. These measurements were repeated twice. The measured beam-energy spectra are shown in Fig. 1. The energy loss of the  $^{48}\text{Ca}$  beam passing through various thicknesses of Be was calculated using the software program "Targetsetup" [37] based on the stopping power code reported in [38]. A linear calibration could be established. Accuracy of about  $\pm 5\%$  is claimed in [39] for the heavy ion stopping calculation of Ti in C which is one of the existing experimental data sets closest to the combination Ca in Be. Subsequently, the beam energy spectrum behind the rotating target setups used in Experiment I was measured. An unexpected energy spectrum with 2 maxima was caused by an uneven distribution of the  $\text{U}_3\text{O}_8$  layer on top of the ba-

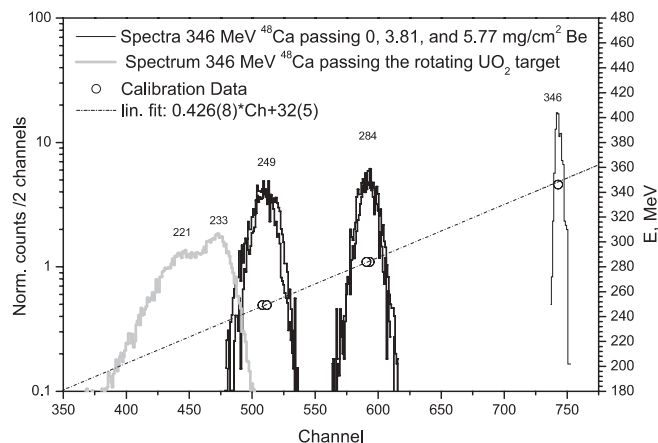


**Fig. 1.** Beam energy spectra measured with a PIPS solid state detector. A  $346\text{ MeV } ^{48}\text{Ca}$  beam was measured directly and after passing  $3.81\text{ mg/cm}^2$  Be and  $5.77\text{ mg/cm}^2$  Be. Residual energies of  $284\text{ MeV}$  and  $249\text{ MeV}$  were expected, respectively [37] and confirmed by measurements repeated two times (black lines). The corresponding energy calibration is indicated (dash-dotted line). In a subsequent experiment the beam was passed through the rotating U-target assembly, consisting of Be-vacuum windows (average thickness:  $3.82\text{ mg/cm}^2$ ) and Be-backings (average thickness:  $2.33\text{ mg/cm}^2$ ) covered with  $^{238}\text{U}_3\text{O}_8$  (average U-thickness:  $1.6\text{ mg/cm}^2$ ) (grey line).

nana shaped segments of the target wheel and a variability in the Be thickness across vacuum window and target backing segments (see Fig. 1). However, these measurements offered the possibility to estimate the beam energy distribution in the target as shown in Fig. 2. To obtain a rough estimate of the effective target thickness, this distribution was folded into a hypothetical excitation function for the  $3n$  evaporation channel in the  $^{48}\text{Ca}$  induced fusion reactions with  $^{238}\text{U}$ . The shape of the excitation function reported in [9] was used. Its maximum was placed at  $232\text{ MeV}$ . At this center-of-target energy the production of the long-lived  $^{283}112$  was reported [11, 12, 26] (see Fig. 2). From the overlap between this hypothetical excitation function and the

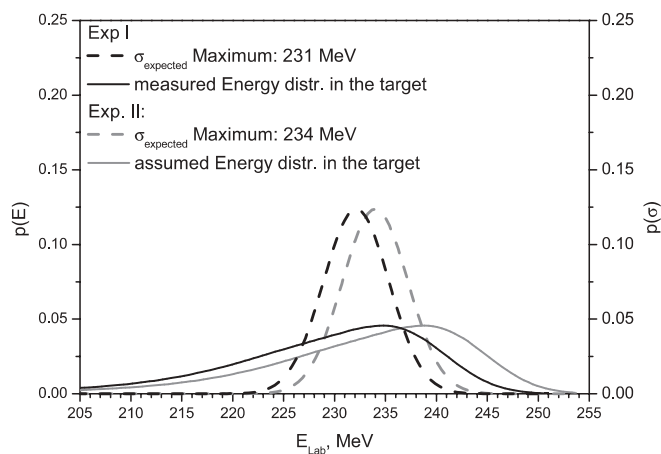


**Fig. 2.** The beam energy distribution in the target material deduced from the measurements of the beam energy distributions in Experiment I (solid black line, left hand scale). The beam energy distribution assumed for Experiment II (solid grey line, left hand scale). The normalized assumed  $3n$  evaporation channel excitation functions for the reaction  $^{48}\text{Ca} + ^{238}\text{U}$  have the shape reported in [9]: for Experiment I in 2003 (dashed black line, right hand scale) the peak cross section was assumed to be at  $232\text{ MeV}$  and for Experiment II in 2004 (dashed grey line, right hand scale) at  $234\text{ MeV}$ .

measured beam energy distribution in the target an effective target thickness of about  $800 \mu\text{g}/\text{cm}^2$   $^{238}\text{U}$  was calculated. During 16.8 days the target was irradiated with an overall beam dose of  $2.8 \times 10^{18}$   $^{48}\text{Ca}$  particles. The COLD detector was placed behind 2.5 m of concrete shielding at an angle of about  $90^\circ$  with respect to the beam axis at the target.

## 2.2 Experiment II

Prior to the Experiment II, extensive efforts were made to improve the IVO-COLD setup to be sensitive to detect  $^{283}112$  independent of its claimed decay properties (long-lived SF or short-lived  $\alpha$ -emitter). A new, smaller recoil chamber was designed, which could be heated to ensure dryness prior to the experiment. It had an overall volume of about 40 ml and was entirely covered with quartz except for a small area for the graphite beam dump. The outlet of this chamber was connected to a quartz column filled with a Ta foil and a quartz wool plug heated up to  $850^\circ\text{C}$  to retain aerosol particles and to act as getter for oxygen or halogen containing species. The small size of the recoil chamber required the use of a carrier gas with higher stopping power. In test experiments at GSI Darmstadt  $^{180-182}\text{Hg}$  isotopes were produced in the nuclear fusion reaction of a 297 MeV (center-of-target energy)  $^{70}\text{Zn}$  beam and a  $310 \mu\text{g}/\text{cm}^2$   $^{114}\text{Sn}$  target. It was found that the  $^{180-182}\text{Hg}$  products recoiling out of the  $^{114}\text{Sn}$  target with the momentum of the  $^{70}\text{Zn}$  beam were completely stopped in a mixture of 70% He and 30% Ar. Because the  $^{283}112$  atoms should recoil from the  $^{238}\text{U}$  target with the smaller momentum of the  $^{48}\text{Ca}$  beam, it was assumed that they would also be stopped in this mixture. A self-drying closed gas loop system was developed to keep the amount of trace gases such as oxygen and water in this carrier gas mixture as low as possible [40]. The volatile species were transported through a PFA<sup>®</sup> capillary (*i.d.* 1.5 mm) to the thermochromatography device COLD.

The COLD detector was also improved. Instead of using single PIN diodes, pairs of PIN diodes ( $10 \text{ mm} \times 8.9 \text{ mm}$ ) were combined with the active surfaces facing each other, forming a rectangular channel with an open cross section of  $8.9 \times 1.6 \text{ mm}^2$ . This arrangement provided almost  $4\pi$ -detection geometry for a species adsorbed on the active detector area. Thus, a higher sensitivity for detecting correlated decay chains of SHE was obtained compared to Experiment I. Especially the possibility to detect coincident SF fragments is an important upgrade, because all decay chains attributed to SHE observed in  $^{48}\text{Ca}$  induced nuclear reactions with actinides are terminated by a SF. Experiment II was again aiming at the investigation of the adsorption of element 112 on a gold surface. Therefore, the detectors on one side of the channel were covered with a 50-nm thick layer of gold by vapor deposition. 32 “sandwiched” detector pairs were mounted into a steel channel. The side with the gold covered detectors was in close contact with a copper rod welded into the steel channel. Along this copper rod, a temperature gradient from  $0^\circ\text{C}$  to  $-187^\circ\text{C}$  was established using thermostat heating on the warm end and liquid nitrogen cryostat cooling on the cold end. The exact temperature of the detector surface with gold was determined via the measurement of the temperature dependence of the resistance of the PIN photodiodes [31, 41]. The chromato-

graphic channel was vacuum-tight over the entire temperature range. It was placed inside a vacuum chamber held at a pressure of  $< 1 \text{ mbar}$ . This was important to keep the setup as dry as possible. A new data acquisition system was developed to operate the 64 spectroscopic channels and to provide an event-by-event spectroscopy in the energy region from 2–200 MeV.

The entire setup was tested in model experiments with short-lived  $^{182-184}\text{Hg}$  and with  $^{219}\text{Rn}$  ( $t_{1/2} = 3.96 \text{ s}$ ). The average overall transport time determined with  $^{219}\text{Rn}$  was 2.2 s [42]. Therefore, the deposition of the volatile element 112 by adsorption on the detector surface would allow for the measurement of  $\alpha$ - or SF-decays with lifetimes between about two seconds up to one day. An overall efficiency of about 95% has been calculated for  $^{185}\text{Hg}$  ( $t_{1/2} = 49 \text{ s}$ ) including transport losses and deposition efficiency. The deposition efficiencies for the Rn isotopes are strongly dependent on their half-lives. The more long-lived isotopes have more time to participate in the reversible adsorption chromatography process. Therefore, the long-lived isotopes may leave the column at the cold end before decaying. The transport efficiency for  $^{220}\text{Rn}$  ( $t_{1/2} = 55.6 \text{ s}$ ) was about 97%, but only about 50% were deposited in the COLD. As expected, for the shorter-lived  $^{219}\text{Rn}$  the deposition efficiency was higher, about 94%, almost the same as for  $^{185}\text{Hg}$ . However, a transport loss of about 35% has to be considered for the short-lived  $^{219}\text{Rn}$ .

During Experiment II the same  $\text{U}_3\text{O}_8$  target ( $1.6 \text{ mg}/\text{cm}^2$   $^{238}\text{U} + (\text{natNd})$ ) as in Experiment I was irradiated with an integral beam dose of  $1.4 \times 10^{18}$   $^{48}\text{Ca}$  particles. The energy in the center of the target was 235 MeV. The shape of the in-target beam energy distribution was assumed to be the same as in Experiment I, but shifted to energies approximately 4 MeV higher than in Experiment I. The excitation function as it was reported for the  $\alpha$ -decaying  $^{283}112$  [9] (see Fig. 2) was used to estimate the effective target thickness to be about  $800 \mu\text{g}/\text{cm}^2$ .

The setup was optimized for detecting a short-lived 4-s  $^{283}112$ . Therefore, the capillary between target and COLD was kept as short as possible, resulting in the detector being placed almost in the beam axis behind a shielding of about 2 m of concrete and about 0.5 m boron paraffin.

## 3. Results and discussion

### 3.1 Experiment I

In this experiment the conditions were optimized for the detection of the 5-min SF-decay of the isotope  $^{283}112$ . The observation of  $^{283}112$  decaying via  $\alpha$ -particle emission with a half-life of 4 s was almost impossible. Moreover, the design of the experiment limits its chemical sensitivity to the observation of the following adsorption properties for volatile species with a half-life of several minutes:  $-\Delta H_{\text{ads}}^{\text{quartz, PFA}} < 70 \text{ kJ}/\text{mol}$ ,  $-\Delta H_{\text{ads}}^{\text{ice}} > 18 \text{ kJ}/\text{mol}$ . In order to observe its adsorption on an ice-free gold surface it has to have an  $-\Delta H_{\text{ads}}^{\text{Au}} > 45 \text{ kJ}/\text{mol}$ . These limits were determined using the kinetic Monte-Carlo approach based on a model of linear gas adsorption chromatography [43] for the description of the gas phase transport through PFA<sup>®</sup> capillaries, the quartz recoil chamber and in the detector channel.

The distribution of  $^{185}\text{Hg}$  and  $^{220}\text{Rn}$  measured along the COLD is depicted in Fig. 3. The adsorption enthalpies ( $\Delta H_{\text{ads}}$ ) of these elements on the different surfaces in the COLD channel were estimated using the Monte-Carlo simulation technique [43]. The spontaneous, diffusion controlled deposition of  $^{185}\text{Hg}$  on the gold surface opposite the first seven detectors allowed to determine a lower limit for  $-\Delta H_{\text{ads}}^{\text{Au}}(\text{Hg})$  of about 80 kJ/mol. This value is in agreement with literature data  $-\Delta H_{\text{ads}}^{\text{Au}}(\text{Hg}) = 98 \pm 3$  kJ/mol [33, 34]. The  $^{220}\text{Rn}$  deposition on the last 5 detectors corresponds to an adsorption enthalpy of  $-\Delta H_{\text{ads}}(\text{Rn}) = 21.5 \pm 1.0$  kJ/mol [33]. This value is lower than the value measured for the adsorption of Rn on gold surfaces  $-\Delta H_{\text{ads}}^{\text{Au}}(\text{Rn}) = 29 \pm 3$  kJ/mol [44]. However, it agrees well with the adsorption enthalpy measured for Rn on ice surfaces of  $-\Delta H_{\text{ads}}^{\text{ice}}(\text{Rn}) = 20 \pm 2$  kJ/mol [45]. The differences between the measured deposition patterns and the simulated deposition patterns are due to the rectangular geometry of the channel, which is described in the simulation as a set of parallel round tubes with 1.6 mm inner diameter [46]. The determined adsorption data for Rn indicate the presence of an ice coverage beginning at temperatures higher than  $-130$  °C. The presence of an ice layer on the coldest diodes in the COLD array is also corroborated by analyzing the time dependent change of the  $\alpha$ -spectra resolution. This analysis yielded evidence of ice formation at temperatures below about  $-90$  °C [33, 34]. This corresponds to the dew point in the helium carrier gas at a water vapor content of about 0.2 ppm. Accordingly, we have to assume an ice layer covering the entire chromatographic surface from detector #22 to #32. Moreover, the chromatography channel was not helium-tight after cooling the cold end to temperatures below approx.  $-160$  °C. At  $-185$  °C, the channel leaked He at a rate of about 200 ml/min into the previously evacuated housing until equal pressures were reached in the housing and the detector channel. Unfortunately, through this leak, traces of water could diffuse into the detector array leading to thick ice coverage along the coldest 4 to 5 detectors, much thicker than expected from the deposition of microgram amounts of water transported by the carrier gas. This is clearly visible in the energy resolution of the  $\alpha$ -spectra of the detectors #30–32 (FWHM

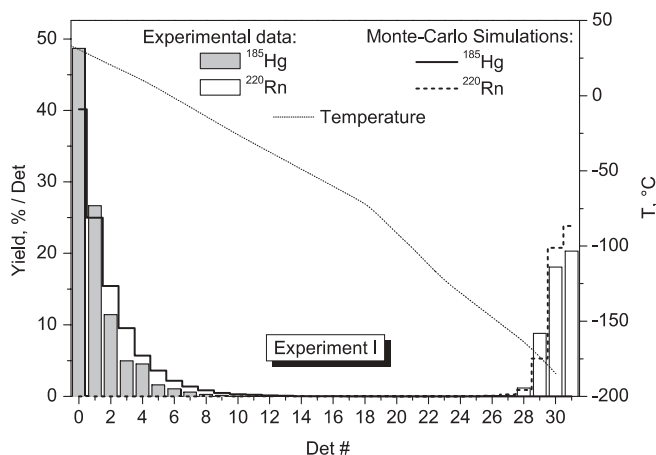


**Fig. 3.** Thermochromatograms of  $^{185}\text{Hg}$  and  $^{220}\text{Rn}$  measured in Experiment I. The Monte-Carlo simulated deposition patterns are indicated, allowing for the determination of adsorption properties of Hg and Rn.

$\sim 150$ – $200$  keV) accumulated during the entire experiment in comparison with the sum spectrum of the detectors #1–10 (FWHM  $\sim 70$  keV) (see Fig. 4). Hence, it can be concluded that traces of water in the carrier gas prevented the adsorption of volatile species on pure gold surfaces below about  $-90$  °C and a severe loss in  $\alpha$ -spectroscopic resolution due to thick ice depositions was observed at temperatures below about  $-150$  °C.

A sum spectrum of all high-energy events is shown in Fig. 5. 20 events were detected above 40 MeV. Only 11 events had energies larger than 50 MeV. The energy calibration was performed with a  $^{252}\text{Cf}$  source measured with an independent PIN photo diode detector at room temperature and using the same data acquisition system. About 95% of all measured SF fragments from  $^{252}\text{Cf}$  had energies above the threshold energy of 50 MeV (Fig. 5). However, the average energy of about 65 MeV for the 11 events recorded during the experiment is significantly lower than expected for SF fragments originating from the SF of

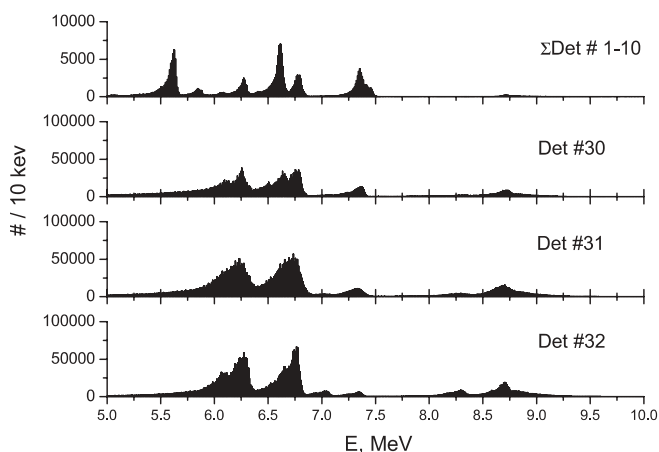


**Fig. 4.** Alpha spectra accumulated throughout the entire Experiment I indicating that the spectroscopic resolution was affected by the ice deposition on detectors 30–32 (three lower spectra). The sum alpha spectrum for the detectors 1–10 is presented for comparison (top spectrum).

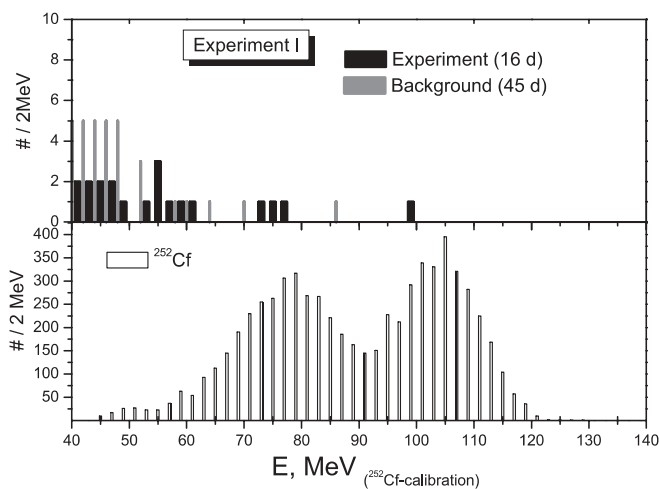


**Fig. 5.** High-energy sum spectrum ( $E > 40$  MeV) measured in the entire 16.8 day irradiation in Experiment I together with the background events detected in 45 d after the irradiation (upper panel). For comparison a  $^{252}\text{Cf}$  SF-spectrum is shown (lower panel) which was measured with the same data acquisition system and a similar PIN diode detector.

<sup>283</sup>112 (TKE  $\sim$  225 MeV [12]). Their energy distribution is markedly different from the expected energy distribution of fission fragments. However, the thick layer – most probably ice – that covered the detector surfaces below  $-150$  °C was expected to severely influence the SF-fragment spectroscopy. Therefore, the events having energies larger than 50 MeV were analyzed for a possible chromatographic behavior. It was found that their distribution along the detector array shows an accumulation of 7 events in the detectors #29–31. This deposition pattern would be expected for a single chemical species. A background measurement was performed for 45 days directly after the experiment using the COLD detector held at room temperature. Only 8 events with  $E > 50$  MeV were observed. These events were randomly distributed along the entire COLD detector (Fig. 6). Using this rate, a total of 3 expected background events in all 32 detectors can be calculated for the duration of the experiment. To test the theory that the high energy events are due to neutron-induced SF of detector material impurities, *e.g.*, <sup>235</sup>U, the measurement of the neutron rate in the vicinity of the target assembly was analyzed. Fluctuations of the neutron flux of about one order of magnitude were measured during the experiment. None of the observed high-energy events occurred during periods of elevated neutron rates. However, the entire background measurement was performed using the COLD detector without cooling and there was no beam on target. Hence, despite the efficient shielding, an increased background count rate during the experiment cannot be ruled out. The analysis of the  $\alpha$ -spectra did not yield any events that might be assigned to a contamination of the detector with heavy actinides. Additionally, during the experiment, the quartz wool filter behind IVO was periodically changed, leached with concentrated nitric acid, and subsequently measured off-line for  $\alpha$ - and SF-events. Peaks of the nuclides <sup>226–228</sup>Th, <sup>224–226</sup>Ac, and <sup>221–228</sup>Ra were observed

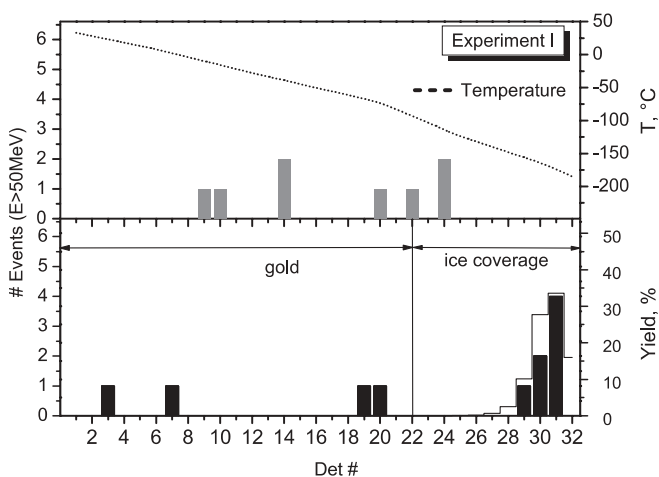


**Fig. 6.** The distribution of the 11 high-energy events ( $E > 50$  MeV) measured along the thermochromatography detector within the 16.8 days of Experiment I. The black line indicates the expected deposition pattern of a volatile species having 5 min half-life and a  $-\Delta H_{\text{ads}}^{\text{ice}} = 25$  kJ/mol (lower panel). The distribution of the 8 background events ( $E > 50$  MeV) measured within 45 days is shown (upper panel). The temperature gradient is indicated (upper panel, black dotted line).

during a counting time of 30 days. No SF-decays were detected.

The following analysis of the gas chromatographic behavior was performed assuming that the high-energy events measured at the cold end of the detector belong to the decay of one single chemical species. By applying the microscopic Monte-Carlo model of gas chromatography, the adsorption enthalpy of the species deposited on the ice layer ( $-\Delta H_{\text{ads}}^{\text{ice}}$ ) is about 25 kJ/mol, assuming its half-life to be 5 min (see Fig. 6). An upper limit for the adsorption enthalpy of this species on gold ( $-\Delta H_{\text{ads}}^{\text{Au}}$ ) of about 50 kJ/mol was estimated, from its observed non adsorption down to a temperature of  $-90$  °C.

Even though Experiment I yielded some indication for a long-lived very volatile species decaying by SF [28], additional confirmation was mandatory with an improved setup that enables the detection of SF coincidences to unambiguously assign the observed decays to element 112.

### 3.2 Experiment II

Apart from the faster transport and separation, an ice-free deposition down to very low temperatures and an almost  $4\pi$ -detection geometry, Experiment II was performed under identical conditions as Experiment I.

The rotating target assembly was overheated during test experiments with <sup>182–184</sup>Hg due to a technical failure of the cooling circuit. As a consequence the gold surfaces of the detectors were contaminated with an unknown organic substance. Despite washing the diodes with methanol, acetone, and diethyl ether, the gold surfaces in the detectors could not be cleaned entirely. Therefore, the deposition pattern of Hg was smeared out over more detectors than anticipated based on Monte-Carlo modeling (see Fig. 7). The energy resolution of the PIN diodes was decreased considerably due to the washing procedure. Therefore, the identification of <sup>185</sup>Hg ( $E_{\alpha} = 5.57, 5.65$  MeV) was hampered by large amounts of <sup>211</sup>At ( $t_{1/2} = 7.2$  h,  $E_{\alpha} = 5.87$  MeV). Much more astatine was measured in this experiment compared

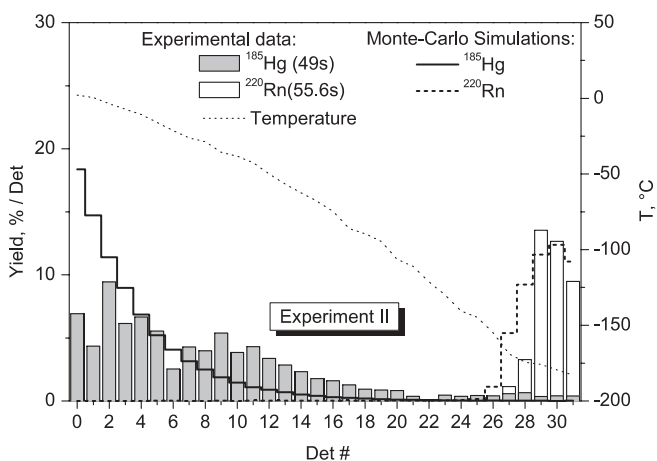


**Fig. 7.** Thermochromatograms of <sup>185</sup>Hg and <sup>220</sup>Rn measured in Experiment II. The Monte-Carlo simulated deposition patterns are indicated, allowing for the determination of adsorption properties of Hg and Rn. The strong disagreement between the simulation and experiment for Hg is due to a contamination of the detector surfaces in the experiment (for details see text).

to Experiment I. This observation may be explained by the use of an Ar/He mixture as carrier gas compared to pure He in the first experiment. Due to the increased stopping power most of the transfer products such as astatine are thermalized in the gas volume of the recoil chamber. Another explanation is the use of the large Ta/Ti metal getter between the recoil chamber and the COLD detector that was used to clean the carrier gas in Experiment I. In this getter, a TiO layer was formed inside the outlet of the getter oven at temperatures between approximately 900 °C and 600 °C. This reactive layer can be expected to irreversibly react with all halogens. In Experiment II this Ta–Ti getter was omitted to minimize the transport time. Only a Ta-foil was inserted into the oven at the outlet of the recoil chamber, which did not efficiently retain the astatine at a temperature of 850 °C. Astatine is known to strongly interact with gold. Hence, as expected, it showed the same diffusion controlled deposition pattern as Hg on the first detectors.  $^{220}\text{Rn}$  showed a deposition maximum on detector #29 (see Fig. 7). The adsorption properties evaluated for Hg and Rn in this experiment are in agreement with the data obtained from Experiment I.  $^{220}\text{Rn}$  ( $-\Delta H_{\text{ads}}^{\text{Au}}(\text{Rn}) = 29 \pm 3 \text{ kJ/mol}$  [44]) was expected to deposit on gold at a temperature of about  $-130^\circ\text{C}$ . Its deposition at the cold end of the detector below  $-150^\circ\text{C}$  is indicative of an ice layer on the detector surfaces beginning at higher temperatures. Hence, it must be concluded that the dew point of water vapor in the carrier gas could not be reduced sufficiently to keep the gold surface clean below approx.  $-100^\circ\text{C}$ . One reason might be that the recoil chamber had to be opened frequently to change the Be-windows. The windows were not able to stand the high-intensity pulsed  $^{48}\text{Ca}$  beam delivered from the UNILAC for more than a few days. However, the resolution of the  $\alpha$ -spectra did not indicate the deposition of large amounts of ice on the detectors within 20 h (see Fig. 8). The resolution of the  $\alpha$ -spectra measured in the entire detector amounted to approx.  $\text{FWHM} = 80\text{--}120 \text{ keV}$  over the entire experiment.

During the experiment, no  $\alpha$ -SF correlations, which would indicate the 4-s  $^{283}112$   $\alpha$ -decaying to the 0.2-s SF activity assigned to  $^{279}\text{Ds}$ , were observed in the  $\alpha$ -energy

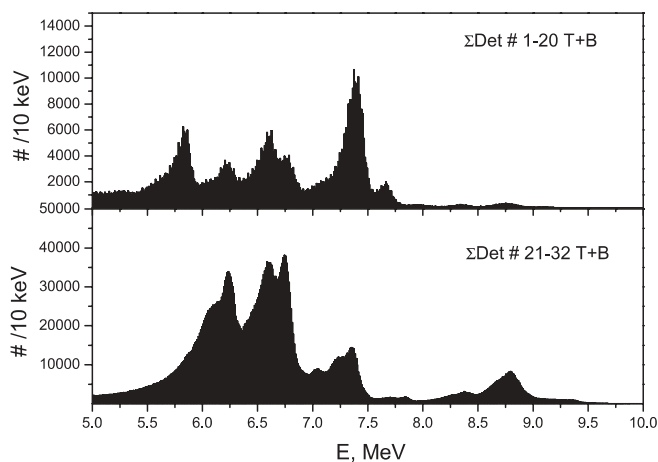


**Fig. 8.** Alpha spectra accumulated throughout the entire Experiment II from top (T) and bottom (B) detectors indicating no difference of the spectroscopic resolution between the first 20 detectors held at temperatures  $> -100^\circ\text{C}$  (upper spectrum) and the 12 detectors held below  $-100^\circ\text{C}$  (lower spectrum).

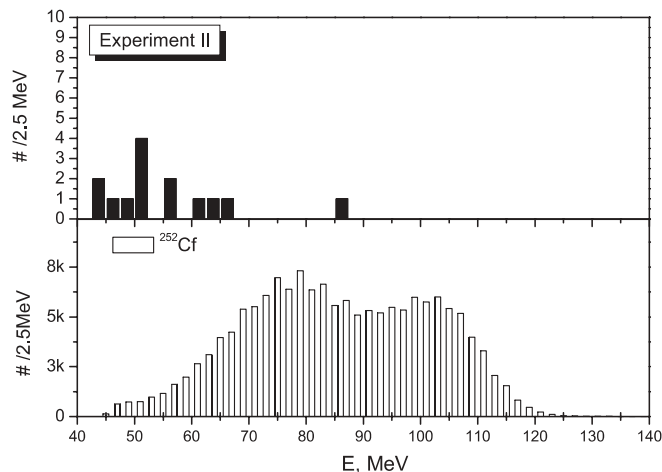


**Fig. 9.** High-energy ( $E > 40 \text{ MeV}$ ) sum spectrum measured in the entire 14 day irradiation of Experiment II (upper panel). The 17 day background measurement did not reveal any event above 40 MeV. For comparison a  $^{252}\text{Cf}$  spectrum is shown (lower panel) which was measured with the same data acquisition system and a similar PIN diode detector.

window between 9.0 and 10.0 MeV in a time window of 3 s. No coincident SF signals were detected. We observed 10 high-energy single events ( $E > 50 \text{ MeV}$ ) in the detectors (see Fig. 9, upper panel) with no preceding  $\alpha$ -decay in the energy range 9.0–10.0 MeV within a time interval of 3 s, which is more than ten times the reported half-life of  $^{279}110$  [9]. The measured energies were compared to a SF spectrum of  $^{252}\text{Cf}$  (see Fig. 9, lower panel) which was measured with the same  $\alpha$ -SF-spectroscopy setup and a separate PIN diode. The distribution of high-energy events along the thermochromatography detector array is presented in Fig. 10. No significant accumulation is observed. During the background measurement without beam and with the COLD detector held at room temperature, no such high-energy events were registered within 17 days. Again, due to the lower than expected energies, and the lack of SF-coincidences (despite the almost  $4\pi$  detection geometry),

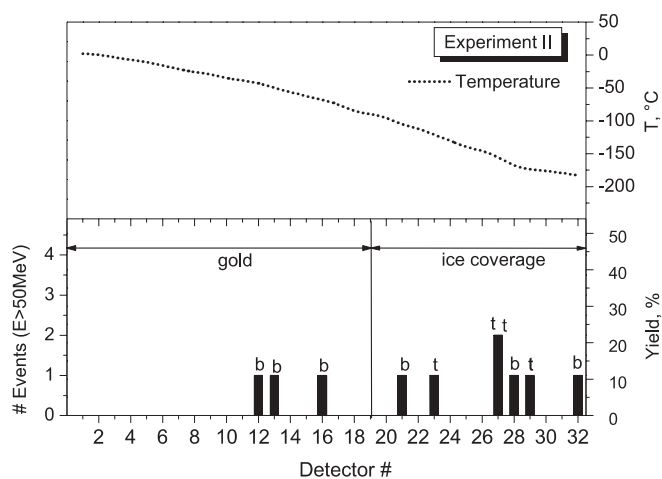


**Fig. 10.** The distribution of the 10 high-energy events ( $E > 50 \text{ MeV}$ ) measured along the thermochromatography detector within the 14 days of Experiment II (lower panel). The detector position top (gold plated) and bottom (standard  $\text{Si}_3\text{N}_4$ ) are indicated by letters  $t$  and  $b$ , respectively. The temperature gradient is shown (upper panel, black dotted line).

these single events cannot be considered unambiguous candidates for any SF-decaying nucleus.

### 3.3 Monte-Carlo calculations of the overall efficiencies

The overall efficiency to detect  $^{283}\text{112}$  in both experiments depends on the transport efficiency and on the place where element 112 is assumed to be preferentially adsorbed in the COLD detector. Hence, the overall efficiency is influenced by the chemical behavior of element 112 and its decay properties. A Monte-Carlo code was developed describing the transport, gas phase adsorption chromatography [43], and the detection of  $^{283}\text{112}$  under the given geometrical boundary conditions of the COLD detector. For a hypothetical Hg-like behavior it was assumed that element 112 has the adsorption properties of Hg on gold [33] and on ice [47]. Similar calculations were also performed for a hypothetical more inert and volatile Rn-like element 112, assuming the adsorption properties of element 112 to be the same as for Rn on gold [44] and ice [45].

#### 3.3.1 Experiment I

The calculated deposition patterns for  $^{283}\text{112}$  (5 min, SF) behaving Hg-like or Rn-like in the COLD detector are presented in Fig. 11 (upper panel). The decay losses of  $^{283}\text{112}$  during transport to the detector were calculated using an average transport time of 25 s. Hence, it was estimated that about 94% of Hg-like  $^{283}\text{112}$  are transported and deposited in the detector, while the transport and deposition yield of Rn-like  $^{283}\text{112}$  is only about 42%. In the case of a Hg-like behavior element 112 is expected to be adsorbed entirely on the gold side of the channel opposite to the detectors. If element 112 approaches the ice covered sections in COLD, it is adsorbed evenly distributed over all of the inner surfaces of the detector channel. Due to this, the adsorption position of  $^{283}\text{112}$  influences the detection efficiency for a fragment

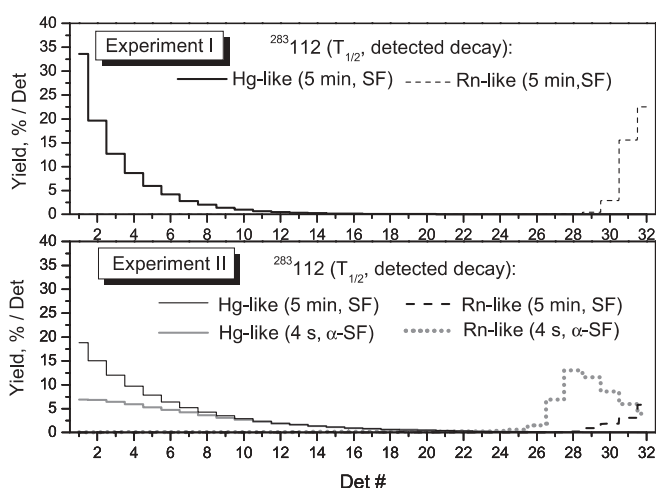


**Fig. 11.** The distributions of  $^{283}\text{112}$  in the thermochromatography detector simulated by the Monte-Carlo method. The calculations include (i) Hg-like or Rn-like behavior, (ii) the detection efficiency for the assumed decay properties indicated in parenthesis, and (iii) the expected transport losses. Regarding the temperature gradients and the ice coverage in the experiments see Figs. 6 and 10.

**Table 1.** Overall efficiencies of the experiments dependent on the decay properties assumed for  $^{283}\text{112}$ , the hypothetical chemical properties for element 112, and the detection efficiencies for correlated and uncorrelated  $\alpha$ , SF<sub>coinc</sub>, and SF<sub>fragment</sub> decay of a species deposited in the COLD detector.

$^{283}\text{112}$ decay ( $t_{1/2}$ )	$\alpha$ -SF <sub>fragment</sub> (4 s)	$\alpha$ -SF <sub>coinc</sub> (4 s)	“Missed $\alpha$ ”-SF <sub>coinc</sub> (4 s)	SF <sub>fragment</sub> (5 min)	SF <sub>coinc</sub> (5 min)
Exp I					
Hg-like	< 0.01			0.616	
Rn-like	< 0.005			0.270	
Exp II					
Hg-like	0.107	0.172	0.165	0.335	0.654
Rn-like	0.105	0.170	0.109	0.104	0.143

from its SF-decay. The overall efficiencies of the experiment were also calculated taking into account all decay properties published so far for  $^{283}\text{112}$ . The results are compiled in Table 1. The overall efficiency of Experiment I to detect  $^{283}\text{112}$  (5 min, SF) by measuring a SF-fragment was 61.6% (being Hg-like) and 27.0% (being Rn-like). The overall efficiency of Experiment I for  $^{283}\text{112}$  (4 s,  $\alpha$ ) is far less than 1%, due to the decay loss during 25 s transport.

The overall efficiency to detect SF-fragments originating from a SF-decaying species with 5 min half-life with an adsorption enthalpy on ice  $-\Delta H_{\text{ads}}^{\text{ice}} = 25$  kJ/mol corresponding to the accumulation of high energy events in Experiment I was calculated as 45.7%.

#### 3.3.2 Experiment II

The Monte-Carlo code used for the data evaluation of Experiment I was adjusted to calculate the overall experimental efficiencies of Experiment II. The calculated deposition pattern of  $^{283}\text{112}$  in the COLD detector depending on its presumed decay properties and chemical behavior are presented in Fig. 11 (lower panel). About 99% of  $^{283}\text{112}$  (Hg-like, 5 min, SF) are transported and deposited in the detector, while the transport and deposition yield of  $^{283}\text{112}$  (Rn-like, 5 min, SF) is only about 28%. A  $^{283}\text{112}$  (Hg-like, 4 s,  $\alpha$ ) is transported and deposited with about 63% yield.  $^{283}\text{112}$  (Rn-like, 4 s,  $\alpha$ ) has a transport and deposition yield of 55%. Element 112 behaving like Hg is assumed to be adsorbed entirely on the gold covered detectors in the channel. In the ice covered region of COLD, element 112 is adsorbed evenly distributed on the detector surfaces and on the side walls of the channel. For the simulation of the chromatographic behavior of the  $^{283}\text{112}$   $\alpha$ -decay daughter  $^{279}\text{Ds}$  its adsorption enthalpies were assumed to be very high on gold and on silica or ice. Hence, every surface hit was calculated to be the final adsorption position of the daughter atom. The calculations considered the possibility that the daughter atoms recoil after the mother  $\alpha$ -decay for 50% of all  $\alpha$ -decays. This consideration has an influence on the calculated detection efficiency of  $\alpha$ -SF correlations. The  $\alpha$ -decay daughter of  $^{283}\text{112}$ ,  $^{279}\text{110}$ , is recoiling up to about 0.3 mm [39] into the carrier gas and is therefore subject to further gas phase transport. Depending on the gas flow dynamics in the chromatographic channel, the decay of the daughter nucleus

might not be correlated anymore with the initial  $\alpha$ -decay of  $^{283}\text{112}$  within a reasonable number of detectors. For this analysis, a decay chain was considered to be correlated, when the alpha particle of  $^{283}\text{112}$  was measured in one detector and the SF-coincidence or SF-fragment of  $^{279}\text{Ds}$  was measured in the same or in either one of the neighboring detector pairs. The small  $\alpha$ -decay branch reported for  $^{279}\text{Ds}$  [9] was neglected. The decay losses during the transport of  $^{283}\text{112}$  to the detector were included in the simulation using a lognormal probability distribution of transport times as it was measured prior to the experiment with  $^{219}\text{Rn}$  (see Fig. 12). The results of these overall-efficiency calculations as a function of the decay properties and of the chemical behavior of  $^{283}\text{112}$  are presented in Table 1. The overall efficiency of Experiment II to unambiguously detect SF-coincidences, correlated  $\alpha$ -SF-fragments, and  $\alpha$ -SF-coincidences originating from  $^{283}\text{112}$  (4 s,  $\alpha$ ) was 44.4% (being Hg-like) and 38.4% (being Rn-like). Experiment II was sensitive also to unambiguously detect  $^{283}\text{112}$  (5 min, SF) by measuring SF-coincidences with an overall efficiency of 65.4% (being Hg-like) and 14.3% (being Rn-like).

The overall efficiency to detect SF-coincidences in Experiment II originating from a SF-decaying species with an adsorption enthalpy on ice of  $-\Delta H_{\text{ads}}^{\text{ice}} = 25$  kJ/mol and 5 min half-life was calculated to 37.8%.

### 3.4 Hypothetical chemical properties of element 112 not covered by the experiments

Experiments I and II were designed to investigate an element 112 having a volatility and reactivity with gold, quartz, or ice between Hg and Rn. However, uncertainties exist in the predicted chemical properties of element 112, which justify the following hypothetical considerations:

If the element 112 interaction with ice is much weaker than Rn, it could still be observed in the chemistry experiments performed at FLNR Dubna but not in the thermochromatographic experiments described in this work. The polarizability of element 112 as predicted in [48] could justify a much weaker adsorption interaction of element 112 with

ice compared to Rn. The physisorption interaction of a hypothetical noble-gas like element 112 on gold being close to that of Xe ( $-\Delta H_{\text{ads}}^{\text{Au}}(\text{Xe}) = 27$  kJ/mol [49]) was predicted in [44] based on the calculated polarizability [48] and ionization potential [50]. However, currently neither experimental data nor predictions exist about energetic quantities of the adsorption interaction of Xe or element 112 on ice.

If element 112 is hypothetically much less volatile compared to Hg, it would be retained during the transport of the products before reaching the thermochromatography detector. However, there is no prediction for such a behavior so far.

In both these hypothetical cases Experiments I and II were not sensitive to detect element 112.

### 3.5 Statistical considerations

A statistical analysis was applied to determine the sensitivity limits reached in both experiments. The Poisson distributed probabilities to observe zero events at hypothetical production cross sections were calculated. The applied beam dose, the target thicknesses, and the overall efficiencies, which are dependent on the assumed decay properties of  $^{283}\text{112}$  and on the chemical properties assumed for element 112 (see Table 1) were used in this calculation. For the calculation of the sensitivity limits the probability distributions were normalized and integrated (see Fig. 13). The deduced sensitivity limits based on a 94.45% statistical confidence level are compiled in Table 2. These upper limit sensitivities represent the production cross section of  $^{283}\text{112}$  in case of having observed 3 unambiguous events.

At 94.45% statistical confidence Experiment I was sensitive to detect the SF-decay of  $^{283}\text{112}$  with a half-life of 5 min formed at a cross section limit of about 0.8 pb (if being Hg-like) and 1.9 pb (if being Rn-like). Experiment II was sensitive to an upper cross section limit of about 2.3 pb or 2.7 pb for a  $^{283}\text{112}$  behaving either similar to Hg or to Rn, respectively, and having a half-life of about 4 s and  $\alpha$ -decaying to a 200 ms

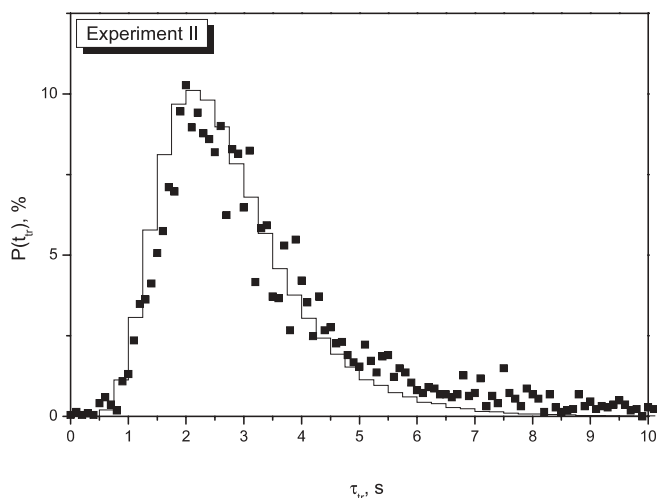


**Fig. 12.** The transport time distribution measured in Experiment II with  $^{219}\text{Rn}$  (black squares) together with the deduced lognormal distribution as used for the transport efficiency calculations (black line).

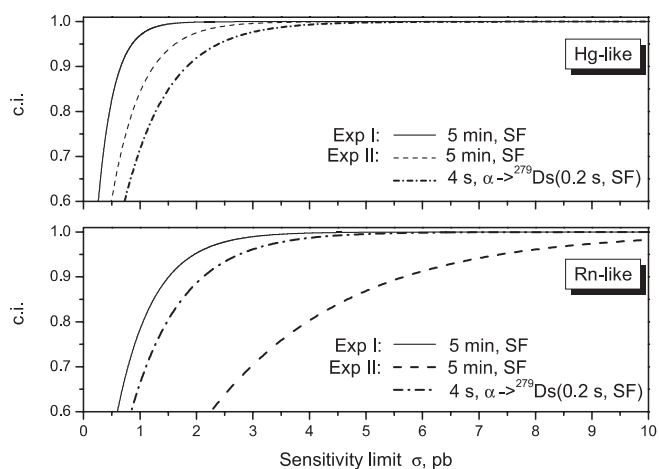


**Fig. 13.** The sensitivity limits of the experiments dependent on the assumption of a Hg-like (upper panel) or Rn-like (lower panel) behavior of element 112 in the chromatography. Separate curves for the different decay properties reported so far for  $^{283}\text{112}$  are shown.

**Table 2.** Results from experiments published so far for  $^{283}112$  produced in the reaction of  $^{48}\text{Ca}$  with  $^{238}\text{U}$  and from this work.  $N$  is the number of observed decays assigned to  $^{283}112$ .

Literature	Beam dose $10^{18}$	Target Thickness (effective) $10^{17}$	Energy (COT) MeV	Decay properties of $^{283}112(t_{1/2})$				$N$
				Overall eff.		Production cross sections, pb		
				$\alpha$ -SF(4 s)	SF(5 min)	$\alpha$ -SF(4 s)	SF(5 min)	
[10, 11]	3.5	7.6	231				$5^{+6.3}_{-3.2}$	2
[12]	4.7	8.9	234				$3^{+4}_{-2}$	2
[9]	7.3	11	234			$2.5^{+1.8}_{-1.1}$		6
[26]	2.8	25	231			$> 7^a$ [27]	$2^{+0.9}_{-0.7}$	8
[13, 14]	1.85	12	230				$< 1.6^b$	0
	2.26	11	236				$< 2.0^b$	0
This work:								
Exp. I								
Hg-like	2.8	20	231	$< 0.01$	0.616	$> 56$	$< 0.8^c$	0
Rn-like	2.8	20	231	$< 0.005$	0.270	$> 112$	$< 1.9^c$	0
Exp. II								
Hg-like	1.4	20	235	0.444	0.654	$< 2.3^c$	$< 1.7^c$	0
Rn-like	1.4	20	235	0.384	0.143	$< 2.7^c$	$< 7.6^c$	0

a: Some of the observed SF-decays in [26] were hypothetically attributed to the less efficient transport of the 4-s  $\alpha$ -decaying  $^{283}112$  followed by SF of the 0.2-s  $^{279}\text{Ds}$  [27];

b: Cross section limits at 84% c.i.;

c: Upper limit sensitivities at 95.45% c.i.

$^{279}\text{Ds}$  (0.2 s, SF). Sensitivity limits of Experiment II for the observation of  $^{283}112$  (SF) with a half-life of 5 min were 1.7 pb (if being Hg-like) and 7.6 pb (if being Rn-like).

Assuming that the 7 observed high-energy events in Experiment I could be assigned to the decay of 5-min  $^{283}112$ , the production cross section of a chemical species with an adsorption enthalpy on ice  $-\Delta H_{\text{ads}}^{\text{ice}} = 25$  kJ/mol could be calculated as  $2.7^{+2.3}_{-1.9}$  pb (95.45% c.i.). The upper limit sensitivity to detect the same species in Experiment II by SF-coincidence was 2.71 pb at 95.45% confidence. The observation of similar high-energy single events with no coincidences in Experiment II, indicate that most of the observed high-energy events in Experiment I were not true SF in contrast to a previous report [28]. All data published so far about the production of  $^{283}112$  in the  $^{48}\text{Ca}$  on  $^{238}\text{U}$  reaction and its decay properties are summarized in Table 2 together with the achieved sensitivity limits of this work. The uncertainties of the chemical properties of element 112 make any estimation of systematic errors of the achieved upper sensitivity limits pointless. Comparison with production cross sections reported in non-chemistry experiments is problematic. However, a comparison to the first chemical experiments with  $^{283}112$  at FLNR Dubna [26] is possible. The initial report on Experiment I [28] seemed to corroborate the observation of a long-lived SF species produced on a 2-pb cross section level and behaving similar to Rn. However, in the more likely case, that in Experiment I no long-lived SF-decaying  $^{283}112$  was observed, the upper cross section limit of about 1.9 pb does not disprove the findings from FLNR Dubna. The sensitivity limit of about 2.5 pb reached in Experiment II for short  $\alpha$ -SF correlations makes it unlikely that the events observed in the FLNR Dubna chemistry experiment originate from short-lived  $\alpha$ -emitting  $^{283}112$  followed by SF of  $^{279}\text{Ds}$  [27].

## 4. Conclusion

Two gas adsorption thermochromatography experiments were performed that were sensitive to detect  $^{283}112$  over a broad range of adsorption properties between its group 12 homologue Hg and the noble gas Rn. Both experiments did not detect any decay pattern that can be unambiguously attributed to a super heavy element. All decay properties reported so far for  $^{283}112$  have been considered. The upper limit sensitivity levels reached in both experiments for the detection of  $^{283}112$  behaving chemically similar to Hg or to Rn are not low enough to significantly contradict the published data on the formation of this isotope in the nuclear fusion reaction of  $^{48}\text{Ca}$  with  $^{238}\text{U}$  or the results of the first chemistry experiments with element 112 reported by FLNR Dubna.

*Acknowledgment.* We thank the crew of the GSI UNILAC and the GSI ECR ion source group for providing intense and stable beams of  $^{48}\text{Ca}$ . We are indebted to the GSI target laboratory for the supply of Be foils for the vacuum windows. Our thanks go to F. Glaus from the Laboratory of Micro- and Nanotechnology of PSI for the preparation of the PIN-diodes and to P. Rasmussen from the Electronics group at PSI for his invaluable help during the development and construction of the new data acquisition electronics for Experiment II. Financial support was provided by the Swiss National Science Foundation Grants 200020-101578/1 and 2000-065050.01, the Office of High Energy and Nuclear Physics, the Nuclear Physics Division of the U.S. Department of Energy, under contract DE-AC03-76SF000988 and grant DE-FG06-97ER41026.

## References

1. Myers, W. D., Swiatecki, W. J.: Nucl. Phys. **81**, 1 (1966).
2. Meldner, H.: Ark. Fys. **36**, 593 (1967).
3. Herrmann, G.: In: *Radiochemistry*. Int. Rev. Sci. Inorg. Chem. Ser. Two, Vol. 8. (Maddock, A. G., ed.) Butterworths, London (1975).
4. Herrmann, G.: In: *Chemistry of Superheavy Elements*. (Schädel, M., ed.) Kluwer Academic Publishers, Dordrecht (2003) Chapt. 8, p. 291.

5. Oganessian, Yu. Ts., Bruchertseifer, H., Buklanov, G. V., Chepigin, V. I., Choi Val Sek, Eichler, B., Gavrillov, K. A., Gäggeler, H. W., Korotkin, Yu. S., Orlova, O. A., Reetz, T., Seidel, W., Ter-Akopian, G. M., Tretjakova, S. P., Zvara, I.: *Nucl. Phys. A* **294**, 213 (1978).
6. Gäggeler, H. W., Trautmann, N., Brüchle, W., Herrmann, G., Kratz, J. V., Peuser, P., Schädel, M., Tittel, G., Wirth, G., Ahrens, H., Folger, H., Franz, G., Sümmerer, K., Zendel, M.: *Phys. Rev. Lett.* **45**, 1824 (1980).
7. Armbruster, P., Agarwal, Y. K., Brüchle, W., Brügger, M., Dufour, J. P., Gäggeler, H., Hessberger, F. P., Hofmann, S., Lemmertz, P., Münzenberg, G., Poppensieker, K., Reisdorf, W., Schädel, M., Schmidt, K. H., Schneider, J. H. R., Schneider, W. F. W., Sümmerer, K., Vermeulen, D., Wirth, G., Ghiorso, A., Gregorich, K. E., Lee, D., Leino, M., Moody, K. J., Seaborg, G. T., Welch, R. B., Wilmarth, P., Yashita, S., Frink, C., Greulich, N., Herrmann, G., Hickmann, U., Hildebrand, N., Kratz, J. V., Trautmann, N., Fowler, M. M., Hoffman, D. C., Daniels, W. R., von Gunten, H. R., Dornhöfer, H.: *Phys. Rev. Lett.* **54**, 406 (1985).
8. Hofmann, S., Münzenberg, G.: *Rev. Mod. Phys.* **72**, 733 (2000).
9. Oganessian, Yu. Ts., Utyonkov, V. K., Lobanov, Yu. V., Abdullin, F. Sh., Polyakov, A. N., Shirokovsky, I. V., Tsyganov, Yu. S., Gulbekian, G. G., Bogomolov, S. L., Gikal, B. N., Iliev, S., Subbotin, V. G., Sikhov, A. M., Voinov, A. A., Buklanov, G. V., Subotic, K., Zagrebaev, V. I., Itkis, M. G., Patin, J. B., Moody, K. J., Wild, J. F., Stoyer, M. A., Stoyer, N. J., Shaughnessy, D. A., Kennaally, J. M., Wilk, P. A., Loughheed, R. W., Il'kaev, R. I., Vesnovskii, S. P.: *Phys. Rev. C* **70**, 064609 (2004).
10. Oganessian, Yu. Ts., Yeremin, A. V., Popeko, A. G., Bogomolov, S. L., Buklanov, G. V., Chelnokov, M. L., Chepigin, V. I., Gikal, B. N., Gorshkov, V. A., Gulbekian, G. G., Itkis, M. G., Kabachenko, A. P., Lavrentev, A. Yu., Malyshev, O. N., Rohac, J., Sagaidak, R. N., Hofmann, S., Saro, S., Giardina, G., Morita, K.: *Nature* **400**, 242 (1999).
11. Oganessian, Yu. Ts., Yeremin, A. V., Gulbekian, G. G., Bogomolov, S. L., Chepigin, V. I., Gikal, B. N., Gorshkov, V. A., Itkis, M. G., Kabachenko, A. P., Kutner, V. B., Lavrentev, A. Yu., Malyshev, O. N., Popeko, A. G., Rohac, J., Sagaidak, R. N., Hofmann, S., Münzenberg, G., Veselsky, M., Saro, S., Iwasa, N., Morita, K.: *Eur. Phys. J. A* **5**, 63 (1999).
12. Oganessian, Y. T., Yeremin, A. V., Popeko, A. G., Malyshev, O. N., Belozero, A. V., Buklanov, G. V., Chelnokov, M. L., Chepigin, V. I., Gorshkov, V. A., Hofmann, S., Itkis, M. G., Kabachenko, A. P., Kindler, B., Münzenberg, G., Sagaidak, R. N., Saro, S., Schött, H.-J., Streicher, B., Shutov, A. V., Svirikhin, A. I., Vostokin, G. K.: *Eur. Phys. J. A* **19**, 3 (2004).
13. Loveland W., Gregorich, K. E., Patin, J. B., Peterson, D., Rouki, C., Zielinski, P. M., Aleklett, K.: *Phys. Rev. C* **66**, 044617 (2002).
14. Gregorich, K. E., Loveland, W., Peterson, D., Zielinski, P. M., Nelson, S. L., Chung, Y. H., Düllmann, Ch. E., Folden III, C. M., Aleklett, K., Eichler, R., Hoffman, D. C., Mahmud, H., Omtvedt, J. P., Pang, G. K., Schwantes, J. M., Sprunger, P., Sudowe, R., Wilson, R. E., Nitsche, H.: *Phys. Rev. C* **72**, 014605 (2005).
15. Pitzer, K. S.: *J. Chem. Phys.* **63**(2), 1032 (1975).
16. Pyykkö, P., Desclaux, J.: *Acc. Chem. Res.* **12**, 276 (1979).
17. Schwerdtfeger, P., Seth, M.: *Encyclopedia of Computational Chemistry*, Vol. 4, Wiley, New York (1998).
18. Pershina, V., Bastug, T., Jacob, T., Fricke, B., Varga, S.: *J. Chem. Phys. Lett.* **365**, 176 (2002).
19. Pershina, V., Bastug, T.: *Chem. Phys.* **311**, 139 (2005).
20. Eichler, B.: *Kernenergie* **19**, 307 (1976).
21. Eichler, B., Rossbach, H.: *Radiochim. Acta* **33**, 121 (1983).
22. Eichler, B.: PSI Report 00-09, Villigen (2000), ISSN 1019-0643.
23. Eichler, B.: PSI Report 03-01, Villigen (2002), ISSN 1019-0643.
24. Eichler, B., Eichler, R.: *In Chemistry of Superheavy Elements*. (Schädel, M., ed.) Kluwer Academic Publishers, Dordrecht (2003) Chapt. 6, p. 205.
25. Yakushev, A. B., Buklanov, G. V., Chelnokov, M. L., Chepigin, V. I., Dmitriev, S. N., Gorshkov, V. A., Hübener, S., Lebedev, V. Ya., Malyshev, O. N., Oganessian, Yu. Ts., Popeko, A. G., Sokol, E. A., Timokhin, S. N., Türler, A., Vasko, V. M., Yeremin, A. V., Zvara, I.: *Radiochim. Acta* **89**, 743 (2001).
26. Yakushev, A. B., Zvara, I., Oganessian, Yu. Ts., Belozero, A. V., Dmitriev, S. N., Eichler, B., Hübener, S., Sokol, E. A., Türler, A., Yeremin, A. V., Buklanov, G. V., Chelnokov, M. L., Chepigin, V. I., Gorshkov, V. A., Gulyaev, A. V., Lebedev, V. Ya., Malyshev, O. N., Popeko, A. G., Soverna, S., Szegłowski, Z., Timokhin, S. N., Tretjakova, S. P., Vasko, V. M., Itkis, M. G.: *Radiochim. Acta* **91**, 433 (2003).
27. Yakushev, A. B., Zvara, I., Oganessian, Yu. Ts., Belozero, A. V., Dmitriev, S. N., Eichler, B., Hübener, S., Sokol, E. A., Türler, A., Yeremin, A. V., Buklanov, G. V., Chelnokov, M. L., Chepigin, V. I., Gorshkov, V. A., Gulyaev, A. V., Lebedev, V. Ya., Malyshev, O. N., Popeko, A. G., Soverna, S., Szegłowski, Z., Timokhin, S. N., Tretjakova, S. P., Vasko, V. M., Itkis, M.: *Chemical Identification and Properties of Element 112*. Extended Abstract, 6<sup>th</sup> Int. Conf. on Nuclear and Radiochemistry (NRC 6), 29 Aug.–3 Sept. (2004) Aachen, Germany, p. 112.
28. Gäggeler, H. W.: *Conf. Proc. 8<sup>th</sup> Int. Conf. on Nucleus-Nucleus Collisions 2003 (NN2003)*, Moscow, Russia. *Nucl. Phys. A* **734**, 208 (2004).
29. Gäggeler, H. W.: *Conf. Proc. 4<sup>th</sup> Int. Conf. on Exotic Nuclei and Atomic Masses 2004 (ENAM2004)*, Callaway Gardens, Georgia USA: *Eur. Phys. J. A* **25**(s01), 583 (2005) (available on-line only).
30. Düllmann, Ch. E., Eichler, B., Eichler, R., Gäggeler, H. W., Jost, D., Piguet, D., Türler, A.: *Nucl. Instrum. Methods A* **479**, 631 (2002).
31. Kirbach, U. W., Folden III, C. M., Ginter, T. N., Gregorich, K. E., Lee, D. M., Ninov, V., Omtvedt, J. P., Patin, J. B., Seward, N. K., Strellis, D. A., Sudowe, R., Türler, A., Wilk, P. A., Zielinski, P. M., Hoffmann, D. C., Nitsche, H.: *Nucl. Instrum. Methods. A* **484**, 587 (2002).
32. Düllmann, Ch. E., Dressler, R., Eichler, B., Gäggeler, H. W., Glaus, F., Jost, D. T., Piguet, D., Soverna, S., Türler, A., Brüchle, W., Eichler, R., Jäger, E., Pershina, V., Schädel, M., Schausen, B., Schimpf, E., Schött, H.-J., Wirth, G., Eberhardt, K., Thörl, P., Trautmann, N., Ginter, T. N., Gregorich, K. E., Hoffman, D. C., Kirbach, U. W., Lee, D. M., Nitsche, H., Patin, J. B., Sudowe, R., Zielinski, P. M., Timokhin, S. N., Yakushev, A. B., Vahle, A., Qin, Z.: *Nature* **418**, 859 (2002).
33. Soverna, S., Dressler, R., Düllmann, Ch. E., Eichler, B., Eichler, R., Gäggeler, H. W., Haenssler, F., Niklaus, J.-P., Piguet, D., Qin, Z., Türler, A., Yakushev, A. B.: *Radiochim. Acta* **93**, 1 (2005).
34. Soverna, S.: PhD-Doctoral thesis, University of Bern, Bern, Switzerland (2004).
35. Dressler, R.: *PSI Sci. Rep. 2002*, Vol. 1, Particles and Matter, 68 (2003).
36. Eichler, R., Soverna, S.: *Phys. Atom. Nucl.* **66**, 1146 (2003).
37. Gebbert, S., Henniger, J.: Software "Targetsetup 1.1" for the determination the stopping ranges of ions in materials, based on [38] (1997).
38. Ziegler, J. F., Biersack, J. P., Littmark, U.: *The Stopping and Range of Ions in Solids*. Pergamon Press, New York (1985).
39. Ziegler, J. F.: *Nucl. Instrum. Methods. B* **219–220**, 1027 (2004).
40. Haenssler, F.: *PSI Sci. Rep. 2003*, Vol. 1, Particles and Matter, 57 (2004).
41. Gasser, M.: *PSI Sci. Rep. 2004*, Vol. 1, Particles and Matter 57 (2005).
42. Haenssler, F.: *PSI Sci. Rep. 2004*, Vol. 1, Particles and Matter, 56 (2005).
43. Zvara, I.: *Radiochim. Acta* **38**, 95 (1985).
44. Eichler, R., Schädel, M.: *J. Phys. Chem. B* **106**, 5413 (2002).
45. Eichler, B., Zimmermann, P., Gäggeler, H. W.: *J. Phys. Chem. A* **104**, 3126 (2000).
46. Düllmann, Ch. E.: PhD-Doctoral thesis, University of Bern, Bern, Switzerland (2002).
47. Bartels-Rausch, T.: PhD-Doctoral thesis, University of Bern, Bern, Switzerland (2003).
48. Seth, M., Schwerdtfeger, P., Dolg, M.: *J. Chem. Phys.* **106**, 3623 (1997).
49. Miedema, A. R., Nieuwenhuys, B. E.: *Surf. Sci.* **104**, 491 (1981).
50. Eliav, E., Kaldor, U., Ishikawa, Y.: *Phys. Rev. A* **52**, 2765 (1995).